Safe Contact-Rich Control under Smoothed Implicit Contact Dynamics

Anonymous Authors

***Abstract*— Controllers for contact-rich tasks are often designed based on smoothed approximated contact dynamics. The smoothing affects both the contact response and the control input generated by the controller. This raises a broader question: does a sharper contact approximation necessarily improve closed-loop behavior?**

We study how safety filters are affected by contact smoothing; specifically, differentiable implicit contact dynamics are considered with central-path smoothing parameter κ. It is demonstrated that although decreasing κ can improve local contact fidelity, it does not necessarily improve safety of the closed-loop system, when control barrier functions (CBFs) are used. To demonstrate this, we use a force-aware safety filter that enforces a discrete-time CBF condition through a local affine approximation of the implicit contact force, with a robust margin estimated from offline rollouts. Across a 1D particle, planar pusher, box pivot, and hopper, we show that sharper contact approximations do not necessarily improve safety, as decreasing κ changes both the contact response and the control input selected by the safety filter. These results suggest that contact smoothing should be treated as both a modeling and a control design choice in contact-rich systems.

I. Introduction

Robotic systems that undergo intermittent contact with the environment are difficult to plan and control as their contact modes change over time [1], [2]. Explicit hybrid contact models often rely on predefined mode sequences or online mode resolution, which becomes cumbersome in complex contact-rich tasks [3], [4]. Implicit contact dynamics offers an attractive alternative by representing contact within a unified framework without explicit mode scheduling. This formulation has enabled trajectory optimization and planning in several recent works [5], [6], [7], [8].

To make contact dynamics compatible with gradient-based methods, recent approaches smooth the underlying complementarity structure to obtain differentiable models [9], [10]. These smoothed formulations have shown strong performance in planning through contact [11], [12], [13]. However, safety-critical control under such approximate models remains relatively unexplored.

Safety guarantees are particularly important in contact-rich tasks involving fragile objects, uncertain contact conditions, and human interaction. Prior work has incorporated force constraints using explicit contact models and CBF-based filtering [14], [15], [16]. However, these approaches largely exploit control-affine structure, whereas implicit contact dynamics is generally non-affine and governed by complementarity constraints. This makes standard CBF formulations difficult to apply directly [17], [18], [19], and existing safety methods for non-affine systems do not directly address this setting [20], [21], [22].

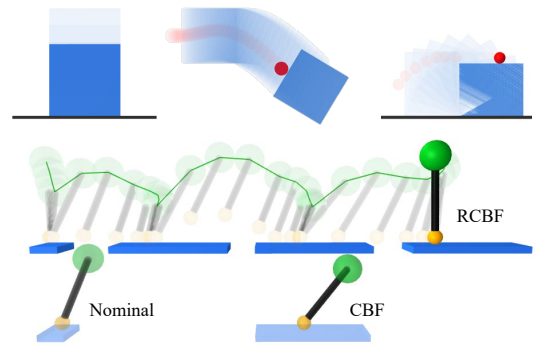

Fig. 1: Overview of the contact-rich control setting and comparison between the nominal CBF and the robust CBF.

Contributions: We study how contact smoothing affects safety-critical control under differentiable implicit contact dynamics. We show that decreasing the smoothing parameter κ does not necessarily improve closed-loop safety, because it alters both the contact response and the filtered control input. To study this interaction in an online safety filter, we locally approximate the implicit contact force and enforce a discrete-time CBF condition through a QP. Building on this formulation, we combine safety-oriented κ selection with a robust offline-estimated margin. Experiments across multiple contact-rich systems show no force violations compared with a standard CBF formulation.

II. Preliminaries and Problem Formulation

We briefly review the implicit contact dynamics model and the discrete-time control barrier functions that form the basis of the proposed safety filter.

A. Contact Dynamics Model

We adopt the complementarity-based implicit contact dynamics model of [10], in which impact and friction are formulated as a Nonlinear Complementarity Problem (NCP).

Here, $\mathcal{Z}$ denotes the configuration space, $\phi : \mathcal{Z} \to \mathbb{R}$ is the signed-distance function, and γ_{k+1} denotes the normal contact impulse at time step $k+1$. In the discrete-time setting, a central-path parameter $\kappa > 0$ relaxes the hard complementarity condition as

$$\phi(z_{k+1}) \geq 0, \tag{1}$$

$$\gamma_{k+1} \geq 0, \tag{2}$$

$$\gamma_{k+1}\phi(z_{k+1}) = \kappa. \tag{3}$$

These conditions enforce non-penetration and unilateral contact while replacing hard complementarity with a smooth central-path relation that is parameterized by κ. Fig. 2 illustrates how κ changes the local sensitivity of the contact

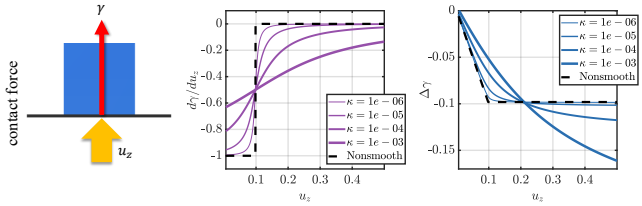

Fig. 2: Gradients for different values of the central-path parameter κ. The dynamics involve a 0.01 kg box resting on a flat surface in the XZ plane, with the applied force increased from 0 N to 0.5 N. γ denotes the contact impulse, and $\Delta\gamma$ its variation with respect to the applied input u_z.

response. In the discrete-time setting, γ_{k+1} can be interpreted as an integrated contact force over one time step.

Friction is modeled through the tangential impulse β_{k+1} and relative tangential velocity v_{k+1} using the maximum dissipation principle

$$\begin{aligned} \min_{\beta_{k+1}} \quad & v_{k+1}^\top \beta_{k+1} \\ \text{s.t.} \quad & \|\beta_{k+1}\|_2 \le \mu \gamma_{k+1}, \end{aligned} \tag{4}$$

where μ is the friction coefficient. The discrete-time contact dynamics are defined implicitly by

$$\mathcal{F}(z_{k-1}, z_k, z_{k+1}, u_k, \gamma_{k+1}, \beta_{k+1}) = 0, \tag{5}$$

together with the unilateral and friction-cone constraints above. We define the problem data and NCP solution variables as

$$\theta_k := (z_{k-1}, z_k, u_k), \quad w_k := (z_{k+1}, \gamma_{k+1}, \beta_{k+1}). \tag{6}$$

The relaxed contact dynamics can be written in residual form as

$$r(w_k; \theta_k, \kappa) = 0, \tag{7}$$

where r stacks the residuals of the discrete-time dynamics and relaxed contact constraints, and

$$w_k^\star := (z_{k+1}^\star, \gamma_{k+1}^\star, \beta_{k+1}^\star). \tag{8}$$

denotes the local solution vector of the relaxed NCP, see [10] for details.

B. Control Barrier Functions

We use the standard discrete-time CBF condition for a system

$$x_{k+1} = f(x_k, u_k), \tag{9}$$

with safe set

$$\mathcal{S} = \{x \mid h(x) \ge 0\}. \tag{10}$$

A discrete-time CBF enforces

$$h(x_{k+1}) - h(x_k) \ge -\alpha h(x_k), \qquad 0 < \alpha \le 1, \tag{11}$$

which implies one-step forward invariance of the set $\mathcal{S}$ [19].

In this work, we study how the central-path parameter κ influences constrained control under implicit contact dynamics. To make this dependence explicit, we consider a force-aware safety filter based on a discrete-time CBF. In this setting, κ affects both the smoothed contact response and the control input selected by the safety filter. Our goal is to understand how this coupling influences closed-loop safety.

III. Safety-Critical Control with Implicit Contact Dynamics

CBF-based safety filters use explicitly defined dynamics to determine safe control inputs and may be implemented as QPs when the dynamics is control-affine. In our setting, however, the contact force is defined implicitly through the NCP solution, and the dynamics are not available in control-affine form. We therefore construct a CBF-based safety filter using a local affine approximation of the implicit contact force.

A. Affine Approximation of the Implicit Contact Force

Since the normal contact force is the primary safety concern in contact-rich control, we define the barrier function as

$$h := F_{\max} - \gamma, \tag{12}$$

where $F_{\max}$ is the maximum allowable contact force. In discrete time, the one-step safety condition from (11) is

$$h_{k+1} \ge (1-\alpha) h_k, \tag{13}$$

where $\alpha \in (0, 1]$ is a design parameter that determines the contraction rate of the discrete-time safety margin.

Let h_{k+1} denote the next-step safety margin, $\hat{h}_{k+1}$ its first-order prediction, and the superscript nom the value at the nominal input. To avoid heavy notation, the dependence on the current state and other problem data is suppressed when it is clear from context. Also, we write the dependence on u_k and κ only when needed.

Because $\gamma_{k+1}(u_k; \kappa)$ is defined implicitly, enforcing (13) directly leads to a nonlinear constrained problem. To obtain a standard CBF-QP, the next-step contact force is linearized around the nominal input u_k^{nom}. With

$$J_{\gamma,k+1} := \left. \frac{\partial \gamma_{k+1}(u_k; \kappa)}{\partial u_k} \right|_{u_k = u_k^{\text{nom}}}, \tag{14}$$

the first-order prediction is

$$\hat{\gamma}_{k+1}(u_k; \kappa) := \gamma_{k+1}^{\text{nom}} + J_{\gamma,k+1}(u_k - u_k^{\text{nom}}), \tag{15}$$

$$\gamma_{k+1}^{\text{nom}} := \gamma_{k+1}(u_k^{\text{nom}}; \kappa). \tag{16}$$

The predicted next-step safety margin is

$$h_{k+1}^{\text{nom}} := F_{\max} - \gamma_{k+1}^{\text{nom}}, \tag{17}$$

$$\hat{h}_{k+1}(u_k; \kappa) = h_{k+1}^{\text{nom}} - J_{\gamma,k+1}(u_k - u_k^{\text{nom}}). \tag{18}$$

Neglecting higher-order terms in the online QP, the safety condition is approximated by

$$J_{\gamma,k+1} u_k \le h_{k+1}^{\text{nom}} + J_{\gamma,k+1} u_k^{\text{nom}} - (1-\alpha) h_k. \tag{19}$$

This yields the CBF-QP

$$u_k^* = \arg\min_{u_k \in \mathcal{U}} \frac{1}{2} \|u_k - u_k^{\text{nom}}\|^2 \quad \text{s.t. (19).} \tag{20}$$

This reformulation enables the use of a standard CBF-QP by addressing the fact that the underlying implicit contact dynamics are not available in explicit form.

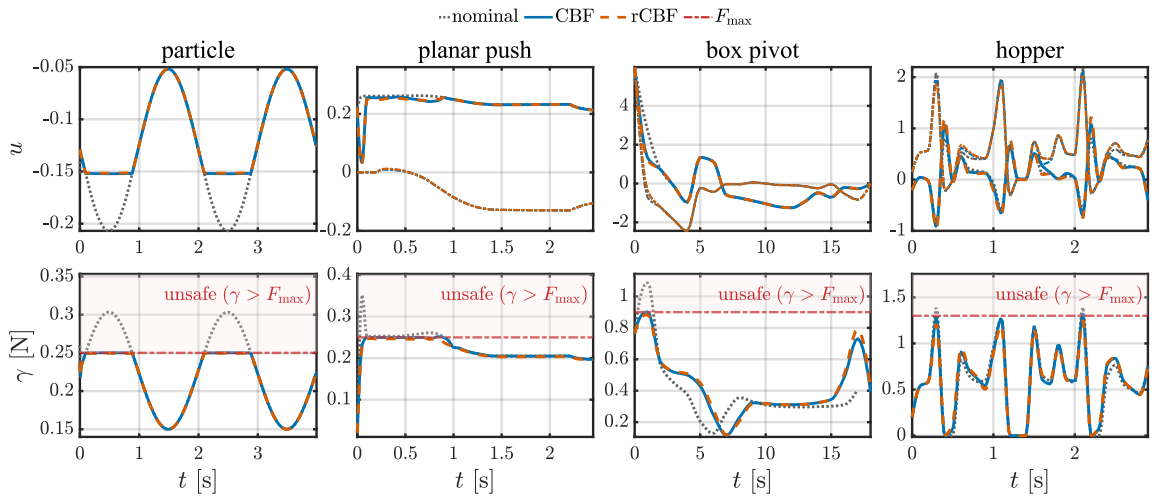

Fig. 3: Control and safety comparison across four systems. The top row shows the control inputs u for the particle, planar pusher, box pivot, and hopper systems (from left to right), while the bottom row shows the corresponding safety metric γ. Black dotted curves denote the nominal controller, blue solid curves denote CBF, and orange dashed curves denote rCBF. The red dash-dotted line indicates $F_{\max}$, and the shaded region marks unsafe operation ($\gamma > F_{\max}$).

B. κ-Dependence of Safety and Practical Design

The central-path parameter κ affects both the smoothed contact map and the control input selected by the safety filter. Thus, decreasing κ does not necessarily improve closed-loop safety monotonically. A local explanation follows from

$$h_{k+1}(\kappa) = F_{\max} - \gamma_{k+1}(u_k^\star(\kappa), \kappa), \tag{21}$$

where $u_k^\star(\kappa)$ denotes the solution of the CBF-QP. Differentiating with respect to κ gives

$$\frac{d}{d\kappa} h_{k+1}(\kappa) = -\underbrace{\frac{\partial \gamma_{k+1}}{\partial u_k}(u_k^\star(\kappa);\kappa)\,\frac{du_k^\star}{d\kappa}}_{\text{optimizer-induced term}} - \underbrace{\frac{\partial \gamma_{k+1}}{\partial \kappa}(u_k^\star(\kappa);\kappa)}_{\text{direct force-map term}}. \tag{22}$$

This shows that κ influences safety both indirectly through the filtered input and directly through the smoothed contact response. Since these terms are not sign-definite in general, decreasing κ does not guarantee monotonic improvement in the true safety margin.

Motivated by this observation, we select κ using a small set of boundary-focused rollouts that drive the closed-loop trajectory near the safety boundary. Candidates are ranked by rollout failure rate, safety violation rate, predicted safety margin, and control deviation, yielding a compact offline selection procedure.

However, the local affine model can still under-predict the loss of safety margin even with a selected κ. To quantify this one-step mismatch, let

$$\Delta h_k := h_{k+1} - \hat{h}_{k+1}. \tag{23}$$

Suppose there exists a constant $\delta_\kappa \geq 0$ that bounds the one-step under-prediction near the safety boundary, in the sense that

$$\Delta h_k \geq -\delta_\kappa. \tag{24}$$

Then enforcing

$$\hat{h}_{k+1}(u_k;\kappa) \geq (1-\alpha)h_k + \delta_\kappa \tag{25}$$

implies

$$h_{k+1} \geq (1-\alpha)h_k. \tag{26}$$

This yields a robust discrete-time CBF with a fixed tightening margin δ_κ that compensates for one-step under-prediction. In practice, δ_κ is chosen conservatively from offline boundary-relevant rollouts using observed under-prediction samples $(-\Delta h_k)^+$.

The tightened condition in (26) guarantees the one-step barrier condition for the smoothed model. This guarantee can be extended to the unsmoothed model by additionally accounting for the smoothing mismatch. Define

$$\Delta h_k^0 := h_{k+1}^0 - h_{k+1}, \tag{27}$$

where h_{k+1}^0 denotes the next-step safety margin under the unsmoothed model. If

$$\Delta h_k \geq -\delta_\kappa, \qquad \Delta h_k^0 \geq -\delta_0, \tag{28}$$

and

$$\hat{h}_{k+1}(u_k;\kappa) \geq (1-\alpha)h_k + \delta_\kappa + \delta_0, \tag{29}$$

then

$$h_{k+1}^0(u_k) \geq (1-\alpha)h_k, \tag{30}$$

since

$$h_{k+1}^0 = \hat{h}_{k+1} + \Delta h_k + \Delta h_k^0 \geq \hat{h}_{k+1} - \delta_\kappa - \delta_0. \tag{31}$$

In practice, only δ_κ is estimated as the implemented safety filter is defined on the smoothed model. The additional term δ_0 is introduced only as an analytical extension, showing how the same tightening argument could be transferred to the unsmoothed model if a bound on the smoothing mismatch were available.

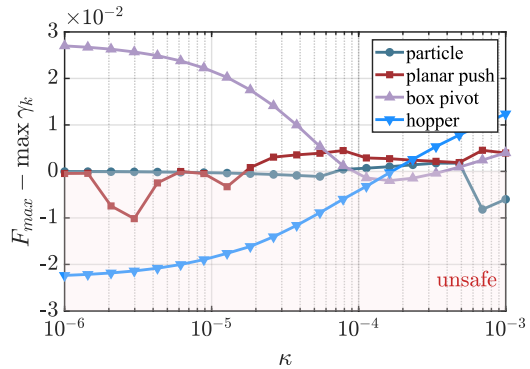

Fig. 4: κ-sweep results across four systems, showing the safety margin with unsafe regions shaded.

IV. Experiments and Results

Four contact-rich systems are used to evaluate the proposed CBF-based safety filtering method under implicit contact dynamics. The experiments are conducted on a 1D particle, a planar pusher, a box pivot, and a hopper, as shown in Fig. 1. All systems use the same force safety constraint, $\gamma \leq F_{\max}$, together with the same implicit contact model and CBF-QP formulation. Reference trajectories are generated by trajectory optimization [23] and tracked by a nominal PD controller without explicit safety enforcement.

A. κ-Dependent Safety Behavior

To study the effect of the central-path parameter κ, we evaluate each system over

$$\kappa \in [10^{-6},\, 10^{-3}], \quad \kappa_i = \mathrm{logspace}(10^{-6}, 10^{-3}, 20), \quad (32)$$

with $\alpha = 0.95$ fixed for all systems.

TABLE I: Quantitative comparison across four systems. Metrics are computed from deterministic rollouts for each controller. The force limits are $F_{\max} = 0.25$ (particle), 0.245 (planar), 0.9 (box pivot), and 1.3 (hopper).

System	Controller	Viol.	Max over.	Peak.	Succ.
Particle	Nominal	0.398	0.0533	0.3033	-
	CBF	0.345	0.0002	0.2502	-
	rCBF	0.000	0.0000	0.2497	-
Planar	Nominal	0.340	0.0799	0.3249	-
	CBF	0.260	0.0000	0.2450	-
	rCBF	0.000	0.0000	0.2450	-
Box pivot	Nominal	0.056	0.1890	1.0890	Y
	CBF	0.053	0.0026	0.9026	N
	rCBF	0.000	0.0000	0.8851	Y
Hopper	Nominal	0.067	0.1017	1.4017	N
	CBF	0.033	0.0117	1.3117	N
	rCBF	0.000	0.0000	1.2225	Y

Fig. 4 shows that the relationship between κ and safety is system-dependent. In many cases, it is non-monotonic. The particle, planar pusher, and box pivot all show non-monotonic trends. Thus, reducing κ does not necessarily improve safety. The hopper shows a monotonic trend over the tested range. Its safety margin increases as κ increases. Still, smaller κ is not necessarily safer. These results suggest that safe κ values often form a range rather than a single best point.

TABLE II: Sensitivity of fixed robust barrier tightening δ_κ on the hopper and planar pusher systems. The columns q_{85} and q_{90} denote the 85th and 90th percentiles of the one-step under-prediction samples $(-\Delta h_k)^+$ used to choose δ_κ, and max denotes the maximum observed under-prediction.

System	Metric	0	q_{85}	q_{90}	max
Hopper	Peak	1.3117	1.2713	1.2560	1.2186
	Viol.	0.033	0.000	0.000	0.000
	Dev.	0.0688	0.0827	0.0866	0.1015
	Succ.	N	Y	Y	Y
Planar	Peak	0.2450	0.2450	0.2450	0.2450
	Viol.	0.260	0.020	0.000	0.000
	Dev.	0.0055	0.0055	0.0055	0.0055
	Succ.	N	N	Y	Y

B. Robust CBF under Approximation Error

Using the κ selected by the boundary-focused procedure, we compare the nominal controller, the standard CBF, and the proposed robust CBF on the same four systems, with $\alpha = 0.95$.

Fig. 3 compares the resulting contact-force trajectories. Table I summarizes the quantitative comparison, where *Viol.* denotes the violation rate, *Max over.* the maximum force overshoot above the limit, *Peak.* the peak contact force, and *Succ.* task success. The standard CBF reduces force violations but does not always eliminate them, since the linearized safety constraint is still affected by approximation error.

By contrast, the proposed robust CBF removes the observed violations in all tested systems and improves task feasibility in the box pivot and hopper, where the standard CBF fails to complete the rollout. Table II shows the trade-off induced by the fixed robust margin δ_κ, where *Dev.* denotes the mean control deviation from the nominal input, measured as $\|u - u^{\mathrm{nom}}\|$. Larger δ_κ improves safety but increases conservativeness. The required margin also depends on the system. In the tested rollouts, q_{85} is sufficient for the hopper, whereas the planar pusher first becomes violation-free at q_{90}.

V. Conclusion

We studied safety-critical control under smoothed implicit contact dynamics and showed that the central-path parameter κ affects both the smoothed contact response and the control input selected by the safety filter. As a result, decreasing κ does not necessarily improve closed-loop safety, even when it improves local contact model fidelity.

Motivated by this, we treated κ as a control-relevant design variable and proposed a boundary-focused κ-selection procedure together with a robust CBF using a tightening margin based on observed one-step under-prediction. The results show that contact smoothing should be understood through its effect on the coupled contact model and control solution in contact-rich systems.

REFERENCES

[1] A. Patel, S. L. Shield, S. Kazi, A. M. Johnson, and L. T. Biegler, "Contact-implicit trajectory optimization using orthogonal collocation," *IEEE Robotics and Automation Letters*, vol. 4, no. 2, pp. 2242–2249, 2019.

[2] F. R. Hogan and A. Rodriguez, "Feedback control of the pusher-slider system: A story of hybrid and underactuated contact dynamics," in *Algorithmic Foundations of Robotics XII: Proceedings of the Twelfth Workshop on the Algorithmic Foundations of Robotics*. Springer, 2020, pp. 800–815.

[3] A. K. Valenzuela, "Mixed-integer convex optimization for planning aggressive motions of legged robots over rough terrain," Ph.D. dissertation, Massachusetts Institute of Technology, 2016.

[4] F. R. Hogan and A. Rodriguez, "Reactive planar non-prehensile manipulation with hybrid model predictive control," *The International Journal of Robotics Research*, vol. 39, no. 7, pp. 755–773, 2020.

[5] M. Posa, C. Cantu, and R. Tedrake, "A direct method for trajectory optimization of rigid bodies through contact," *The International Journal of Robotics Research*, vol. 33, no. 1, pp. 69–81, 2014.

[6] G. Kim, D. Kang, J.-H. Kim, S. Hong, and H.-W. Park, "Contact-implicit model predictive control: Controlling diverse quadruped motions without pre-planned contact modes or trajectories," *The International Journal of Robotics Research*, vol. 44, no. 3, pp. 486–510, 2025.

[7] Y. Shirai, D. K. Jha, and A. U. Raghunathan, "Robust pivoting manipulation using contact implicit bilevel optimization," *IEEE Transactions on Robotics*, vol. 40, pp. 3425–3444, 2024.

[8] H. Lee, Y. Kim, V. M. Staven, and C. Sloth, "Trajectory optimization for in-hand manipulation with tactile force control," *arXiv preprint arXiv:2503.08222*, 2025.

[9] H. J. T. Suh, T. Pang, and R. Tedrake, "Bundled gradients through contact via randomized smoothing," *IEEE Robotics and Automation Letters*, vol. 7, no. 2, pp. 4000–4007, 2022.

[10] T. A. Howell, S. Le Cleac'h, J. Z. Kolter, M. Schwager, and Z. Manchester, "Dojo: A differentiable simulator for robotics," *arXiv preprint arXiv:2203.00806*, vol. 9, no. 2, p. 4, 2022.

[11] T. Pang, H. T. Suh, L. Yang, and R. Tedrake, "Global planning for contact-rich manipulation via local smoothing of quasi-dynamic contact models," *IEEE Transactions on robotics*, vol. 39, no. 6, pp. 4691–4711, 2023.

[12] H. T. Suh, T. Pang, T. Zhao, and R. Tedrake, "Dexterous contact-rich manipulation via the contact trust region," *The International Journal of Robotics Research*, p. 02783649251398875, 2025.

[13] V. Kurtz, A. Castro, A. Ö. Önol, and H. Lin, "Inverse dynamics trajectory optimization for contact-implicit model predictive control," *The International Journal of Robotics Research*, vol. 45, no. 1, pp. 23–40, 2026.

[14] X. Wang, J. Yang, J. Mao, S. Li, and Y. Yan, "Guarding force: Safety-critical compliant control for robot-environment interaction," *IEEE Robotics and Automation Letters*, vol. 11, no. 1, pp. 930–937, 2025.

[15] F. Vinter-Hviid, C. Sloth, T. R. Savarimuthu, and I. Iturrate, "Safe contact-based robot active search using bayesian optimization and control barrier functions," *Frontiers in Robotics and AI*, vol. 11, p. 1344367, 2024.

[16] Y. Kim, J. Kim, A. H. Li, A. D. Ames, and C. Sloth, "Robust adaptive safe robotic grasping with tactile sensing," in *2025 European Control Conference (ECC)*. IEEE, 2025, pp. 2531–2538.

[17] A. D. Ames, S. Coogan, M. Egerstedt, G. Notomista, K. Sreenath, and P. Tabuada, "Control barrier functions: Theory and applications," in *2019 18th European control conference (ECC)*. Ieee, 2019, pp. 3420–3431.

[18] A. Agrawal and K. Sreenath, "Discrete control barrier functions for safety-critical control of discrete systems with application to bipedal robot navigation." in *Robotics: Science and Systems*, vol. 13. Cambridge, MA, USA, 2017, pp. 1–10.

[19] J. Zeng, B. Zhang, and K. Sreenath, "Safety-critical model predictive control with discrete-time control barrier function," in *2021 American Control Conference (ACC)*. IEEE, 2021, pp. 3882–3889.

[20] T. D. Son and Q. Nguyen, "Safety-critical control for non-affine nonlinear systems with application on autonomous vehicle," in *2019 IEEE 58th Conference on Decision and Control (CDC)*. IEEE, 2019, pp. 7623–7628.

[21] J. Seo, J. Lee, E. Baek, R. Horowitz, and J. Choi, "Safety-critical control with nonaffine control inputs via a relaxed control barrier function for an autonomous vehicle," *IEEE Robotics and Automation Letters*, vol. 7, no. 2, pp. 1944–1951, 2022.

[22] W. Xiao, R. Allen, and D. Rus, "Safe neural control for non-affine control systems with differentiable control barrier functions," in *2023 62nd IEEE Conference on Decision and Control (CDC)*. IEEE, 2023, pp. 3366–3371.

[23] T. A. Howell, S. Le Cleac'h, S. Singh, P. Florence, Z. Manchester, and V. Sindhwani, "Trajectory optimization with optimization-based dynamics," *IEEE Robotics and Automation Letters*, vol. 7, no. 3, pp. 6750–6757, 2022.